

Article

Coupling Effect of Space-Arrangement and Wall Thermal Resistance on Indoor Thermal Environment of Passive Solar Single-Family Building in Tibet

Xiaoling Cui, Yangkai Zhang, Guochen Sang *, Wenkang Wang, Yiyun Zhu and Lei Zhang

School of Civil Engineering and Architecture, Xi'an University of Technology, Xi'an 710048, China

* Correspondence: sangguochen@xaut.edu.cn

Received: 1 August 2019; Accepted: 22 August 2019; Published: 2 September 2019



Abstract: In areas where solar energy is abundant, such as the Tibetan plateau, passive solar buildings are attracting more and more attention and becoming a popular form of rural building. However, it is often difficult to achieve the satisfactory indoor thermal environment in a local rural passive solar single-family house. In order to improve the indoor thermal environment of passive solar buildings through building design, a systematic study of rural single-family buildings in Tibet was conducted. The basic parameters were investigated on the outdoor thermal environment, space-arrangement, envelope structure, and the indoor thermal environment. The building model considering space-arrangement modes was developed based on the survey data in multi-space passive solar buildings. The general physical and mathematical analysis models of multi-space passive solar buildings were established based on the heat transfer theory. Furthermore, the effects of space-arrangement and exterior wall thermal resistance on indoor air temperature were analyzed by numerical simulation. Results show that the indoor air temperature of the passive solar building is influenced by space-arrangement and wall thermal resistance together. When the space-arrangement of the building model was changed from “north-south through type” (mode *a*) to “through and separation combination” (mode *b*) and “north-south separation” (mode *c*), the indoor air temperature of the living room increased from 8.8 °C to 10.6 °C and 11.6 °C, with increases of 20.5% and 31.8%, respectively. In addition, equally increasing the thermal resistance of exterior walls in different orientations has different effects on the indoor air temperature. In the space-arrangement mode *c*, comparing with the temperature increment of the living room and bedroom caused by increasing thermal resistance of the south wall and north wall, the temperature increment of the living room caused by increasing thermal resistance of the east/west wall increased by 151.7% and 32.7%, and that of the bedroom increased by 609.1% and 239.1% respectively. This study can provide a reference for the optimal design of passive solar buildings in solar energy abundant areas.

Keywords: passive solar building; indoor space-arrangement; wall thermal resistance; coupling effect; Tibetan Plateau

1. Introduction

There is a growing concern over energy supply and ecological environment conservation in the world. Utilizing a renewable, safe, and eco-friendly energy resource to cater the energy demand of buildings has undoubtedly been regarded as an encouraging solution to achieve sustainable development for buildings.

The Tibet plateau has a peculiar environment, which is characterized by high altitude of over 4000 m, low air temperatures, and transparent and rarified atmosphere with minimal water and dust content. This region has inexhaustible resources of solar energy for annual solar radiation intensity

of approximately 8400 MJ/m² and annual sunshine duration of more than 3000 h [1]. However, the ecological environment is fragile, and conventional fossil energy sources such as coal, oil, and natural gas are very scanty in Tibet. The energy consumption for cooking and heating is dominated by traditional biomass fuel, such as dung, firewood, and crop straw in this region. Excessive depletion of biomass fuel is responsible for eco-environmental degradation [2–4]. It is urgent to develop the non-polluting and renewable energy sources, such as solar energy, to sustain the development of buildings and protect the fragile ecosystem in Tibet [5,6]. Solar buildings utilizing the locally abundant solar energy resources are the most suitable strategy to improve the indoor thermal environment of residential buildings [7,8]. The reported results of local solar radiation estimation [9] and developed passive solar technologies [10–13] make it possible to utilize solar energy to cater to the energy needs of building heating.

A passive solar building is considered to be a promising form suitable for Tibet, which is characterized by a simple structure, high heat collection efficiency, and low construction cost [14–16]. Huang et al. [17] and Liu et al. [18] investigated the influence of conventional passive design methods on the indoor thermal environment. Kirankumar and Wang et al. [15,19] analyzed the effect of external window types and thermal performance of the envelope on the indoor thermal environment of passive solar building. However, it is worth noting that the above research is based on the assumption that the building interior space is a single space. Although assuming the building interior space as a homogeneous whole can simplify the building design, this hypothesis ignores the difference of the thermal environment between different rooms, making it challenging to achieve passive solar building optimization design.

The indoor thermal environment of passive solar buildings is established mainly by the amount of solar energy collected through passive solar technologies and indoor auxiliary heat. Published research on the indoor thermal environment of multi-space buildings indicated that the indoor air temperature of each independent room was different [20]. If the collected solar energy is distributed evenly in every room of the building, the low indoor air temperature of the main room will inevitably occur [21]. Therefore, according to the thermal environment requirement of different rooms, differentially distributing indoor thermal energy is an effective way to improve the efficiency of thermal energy utilization and to raise the indoor air temperature of the main room. The rational layout of the passive solar building with temperature buffers can lead to less heating consumption than the linear layout of the traditional buildings [22]. The temperature buffer is usually served by auxiliary rooms such as kitchens, bathrooms, and storage rooms. Research on the dwelling in Lhasa indicated that the average temperature in south-facing rooms was higher than that in north-facing rooms, and the indoor air temperature of the traditional dwelling was low and fluctuated sharply [23]. As mentioned above, the arrangement of indoor space had a significant effect on the solar energy utilizing efficiency and the indoor thermal environment of passive solar buildings. Rural buildings in the Tibet plateau are generally built of adobe blocks, earth, stone, wood, brick, and concrete block, and the thermal performance of the envelope is generally inadequate. It is difficult to obtain an ideal indoor thermal environment in winter only by habitual construction technology or passive solar technology [20,24–26].

Generally, in the heat transfer analysis of the building envelope, the outdoor air temperature is regarded as the external boundary condition, and the heat transfer modification coefficient is adopted to modify the heat transfer amount of the envelope caused by solar radiation. The heat transfer coefficient of all orientation envelopes is usually constant in building thermal design [27]. However, for areas with high solar radiation intensity, there is the considerable difference of solar radiation intensity in different orientations. If the same heat transfer coefficient is applied to the wall design for all orientations, though this can simplify the thermal design and construction of the wall, it neglects the influence of solar radiation difference in different directions on wall heat transfer, and is not effectively conducive to the optimization of the energy-efficient wall. Sang et al. [28] proposed the design method of “no-uniformity insulation envelope” based on the difference of solar radiation thermal action in the separate direction of the envelope to improve the indoor thermal environment. Nevertheless, the above

method of no-uniformity insulation envelope configuration was built on a single-space solar building. The heat transfer process of multi-space solar buildings is more complicated than that of single-space buildings. It was indicated that the external boundary thermal conditions varied with the orientation, and an open thermodynamic system which had energy exchanges with the outer surroundings and adjacent spaces in multi-space buildings [29,30]. In other words, in the multi-space solar building, there existed simultaneously diversified indoor and outdoor thermal boundary conditions, and heat transfer between the indoor and outdoor, and between adjacent indoor spaces. Obviously, thermal resistance change of exterior walls in different directions has diverse effects on the indoor thermal environment. The renovation that effectively combines the optimization of the wall thermal performance and the indoor space-arrangement is a useful idea to improve the indoor thermal environment in the passive solar building in winter. However, related research has been scarcely reported.

In this paper, we present results from the field survey and measurement designed to obtain the characteristics of residential buildings and the climatic characteristics in the Lhasa area. Based on the local climatic and building feature, the mathematical models of the multi-space solar buildings were established. The coupling influences of indoor space-arrangement and exterior wall thermal resistance on the indoor thermal environment of multi-space solar building were analyzed. In view of the fact that the indoor air temperature is a key parameter for characterizing the indoor thermal environment, in order to simplify the analysis and evaluation, in this study, the indoor air temperature was adopted as an indoor thermal environment evaluation parameter. The result of this study can provide reference for the optimization of solar building thermal design.

2. Indoor and Outdoor Thermal Environment

2.1. Field Survey and Testing of Solar Buildings

The winter in Lhasa is cold and the local residential buildings are in the heating period from November 15th to March 15th of the following year. To obtain the characteristics and current situation of the local solar houses in the Lhasa area, a field survey was conducted from December 26 to 30, 2016. A typical local single-story rural single-family house (Figure 1) was selected to be tested and surveyed in Lhasa area. The testing building is a traditional north-south oriented passive solar building. The main rooms are located in the south, and the auxiliary rooms in the north. The building envelope parameters were measured, as well as the space layout, indoor and outdoor thermal environment, etc. The survey results show that the 500 mm thick adobe walls delimit the indoor and outdoor space, the living room and the kitchen are separated by a thin plate, and the remaining inner partition walls are 500 mm thick adobe walls. Single glazed windows and wooden doors are used and the exterior walls are painted white. The window-to-wall ratios for the south, east, and north directions are 0.42, 0.20, and 0.10, respectively.



Figure 1. Images of the measured rural building in Tibet.

A field measurement was conducted to obtain the indoor and outdoor thermal environment parameters. For the indoor air temperature measurement, the position of the room center 1.5 m from floor was selected as the representative measurement point. The location of the measurement point of the outdoor thermal environment parameter was set in an open space near the testing building. More specifically, the test point of the outdoor air temperature was placed at a position that was not exposed to sunlight and was at a height of 1.5 m from the ground. Measurement of solar radiation intensity was carried out in an open space without any shade. The measuring points of the indoor air temperature were arranged as shown in Figure 2.

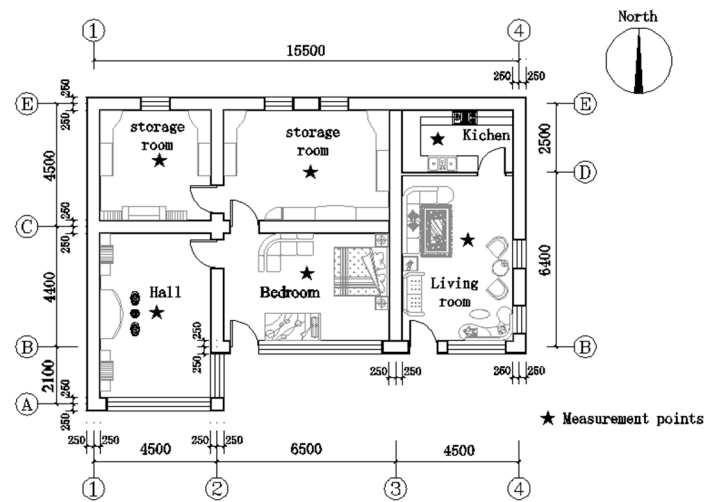


Figure 2. Schematic diagram of the testing building and test point location.

A 175-H1 type self-recording high precision temperature meter with an accuracy of 0.1 °C was selected for the measurement of the indoor and outdoor air temperature. All the indoor and outdoor thermal environment parameters were measured and recorded every 10 min. The geometric sizes of building and envelope were measured using a laser distance meter. The main information about the testing process is shown in Table 1.

Table 1. Main information about the testing.

Survey Content	Main Parameters	Test Duration	Measuring Instruments (Types/Accuracy)	Recording Time Internals
Indoor thermal environment	Air temperature	120 h	Self-recording high precision temperature meter (175-H1/0.1 °C)	10 min
	Air temperature	120 h	Self-recording high precision temperature meter (175-H1/0.1 °C)	10 min
Outdoor thermal environment	Total solar radiation	120 h (Daytime)	Solar radiometer (JTDL-4/±2%)	1 h
	Scattered solar radiation	120 h (Daytime)	Solar radiometer (JTDL-4/±2%)	1 h
Building space and envelope	Geometric size	/	laser distance meter (D510/0.5 mm)	/

2.2. Test Results and Analysis

2.2.1. Outdoor Thermal Environment

The outdoor thermal environment mainly includes outdoor air temperature and solar radiation intensity. The average diurnal variation of solar radiation intensity and the outdoor air temperature over the testing period is shown in Figures 3 and 4.

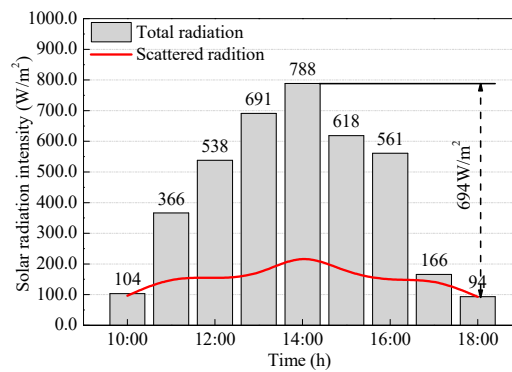


Figure 3. Solar radiation intensity.

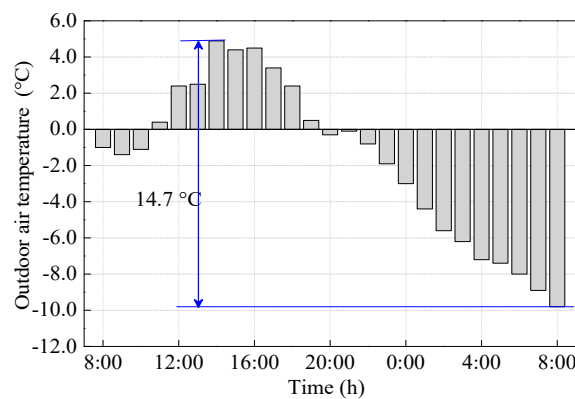


Figure 4. Outdoor air temperature.

As shown in Figure 3, the average sunshine duration is approximately 9 h per day in the test period, and the average radiation intensity is 436 W/m^2 . The highest solar radiation intensity is high up to 788 W/m^2 at 14:00 pm. The proportion of scattered radiation to total radiation is approximately 35%. Figure 4 presents that the average, the highest, and the lowest outdoor air temperature are $-1.7 \text{ }^\circ\text{C}$, $4.9 \text{ }^\circ\text{C}$, and $-9.8 \text{ }^\circ\text{C}$, respectively. Outdoor air temperature fluctuated significantly during the testing day, with a range of $14.7 \text{ }^\circ\text{C}$.

The measured results indicate that, in the Lhasa area, the solar radiation intensity is high, the sunshine duration is long, and the outdoor air temperature fluctuates significantly, but the outdoor air temperature is not too low. It is an ideal climatic condition for passive solar buildings to use solar energy to meet the heat need for winter heating [31].

2.2.2. Indoor Thermal Environment

The average diurnal variation of indoor air temperature in each room over the testing period is illustrated in Figure 5. It is obvious that the indoor air temperatures in the living room and kitchen with auxiliary heat sources are higher than those of other rooms without auxiliary heat sources. The indoor air temperature in the living room and the kitchen fluctuates from $9.0 \text{ }^\circ\text{C}$ to $13.5 \text{ }^\circ\text{C}$, and $7.5 \text{ }^\circ\text{C}$ to $12.0 \text{ }^\circ\text{C}$. The indoor air temperature in the hall and bedroom varies in the range of $6.3 \text{ }^\circ\text{C}$ to $10.7 \text{ }^\circ\text{C}$, and $6.4 \text{ }^\circ\text{C}$ to $11.1 \text{ }^\circ\text{C}$. The indoor air temperature in the storage room in the west and middle fluctuates from $1.9 \text{ }^\circ\text{C}$ to $4.5 \text{ }^\circ\text{C}$, and $3.5 \text{ }^\circ\text{C}$ to $5.3 \text{ }^\circ\text{C}$, respectively.

The frequency distributions of the indoor air temperature segments in all rooms are illustrated in Figures 6 and 7. For rooms without auxiliary heat supply, it can be seen from Figure 6 that the indoor air temperatures of the south-facing rooms (hall, bedroom) are higher than those in the north-facing rooms (storage rooms). Figure 7 demonstrates that, in the absence of auxiliary heat supply, the indoor air temperatures of the south-facing rooms (hall, bedroom) are above $7 \text{ }^\circ\text{C}$ with almost 80% frequency and those in the north-facing rooms (two storage rooms) are below $5 \text{ }^\circ\text{C}$ with the similar frequency.

The above phenomena are ascribed to the north-facing room as “temperature buffer” of the south-facing rooms [32]. The “temperature buffer” effectively reduces the heat transfer losses of the south-facing rooms. The above results show that the difference in ambient conditions of different orientations leads to a significant temperature difference between main and auxiliary rooms in the multi-space solar building. It is worth noting that the indoor air temperatures are low in the testing building. The survey results show that local residents have a good adaptability to such low indoor temperature, but also show an urgent desire to improve the indoor thermal environment.

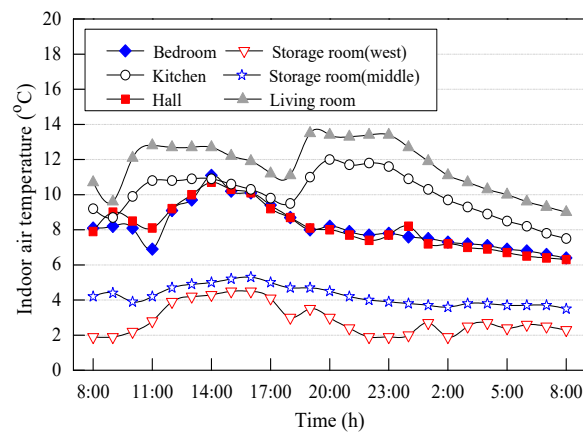


Figure 5. Indoor air temperature.

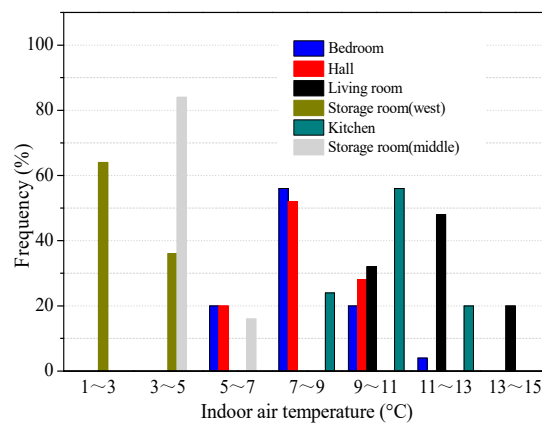


Figure 6. Frequency distribution of the indoor air temperature segments.

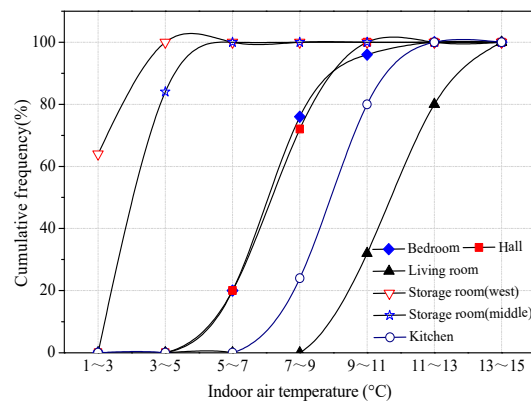


Figure 7. Cumulative frequency distribution of the indoor air temperature segments.

3. Physical and Mathematical Model

The annual heating period of residential buildings in Lhasa is from 15 November to 15 March of the following year, and January is the coldest month. Based on the data obtained from the survey, the building analysis models were proposed, and the mathematical analysis models of the passive solar building were established. Subsequently, the effects of space-arrangement and wall thermal resistance on the indoor air temperature in the coldest month were analyzed by software.

3.1. Building Analysis Model

According to the typical spatial layout and the evolution of rural buildings in the Lhasa area [33], three types of indoor space-arrangement modes were derived and shown in Figure 8 as the building analysis models. In Figure 8, mode *a* is “north-south through” type, mode *b* is “transfixion and separation combination” type and mode *c* is “north-south separation” type. Among them, mode *a* and mode *b* represent the transitional modes in the development of indoor space-arrangement of local rural buildings, while mode *c* represents the current space-arrangement of the modern rural building. The height of the room in all modes is 3.3 m and the parameters of the space-arrangement modes are shown in Table 2.

Table 2. Parameters of space-arrangement modes.

Room	Parameter	Arrangement Mode		
		Mode <i>a</i>	Mode <i>b</i>	Mode <i>c</i>
Bedroom 1	Width/m	5.4	5.4	5.4
	Depth/m	8.1	8.1	5.4
	Space-volume ratio/%	33.3	33.3	22.2
	Orientation Position	South-North West	South-North West	South West
Bedroom 2	Width/m	5.4	5.4	5.4
	Depth/m	8.1	8.1	5.4
	Space-volume ratio/%	33.3	33.3	22.2
	Orientation Position	South-North East	South-North East	South East
Living room 3	Width/m	5.4	5.4	5.4
	Depth/m	8.1	5.4	5.4
	Space-volume ratio/%	33.3	22.2	22.2
	Orientation Position	South-North Middle	South Middle	South Middle
Kitchen 4	Width/m	/	5.4	5.4
	Depth/m	/	2.7	2.7
	Space-volume ratio/%	/	11.1	11.1
	Orientation Position	/	North Middle	North Middle
Storage room 5	Width/m	/	/	5.4
	Depth/m	/	/	2.7
	Space-volume ratio/%	/	/	11.1
	Orientation Position	/	/	North West
Storage room 6	Width/m	/	/	5.4
	Depth/m	/	/	2.7
	Space-volume ratio/%	/	/	11.1
	Orientation Position	/	/	North East

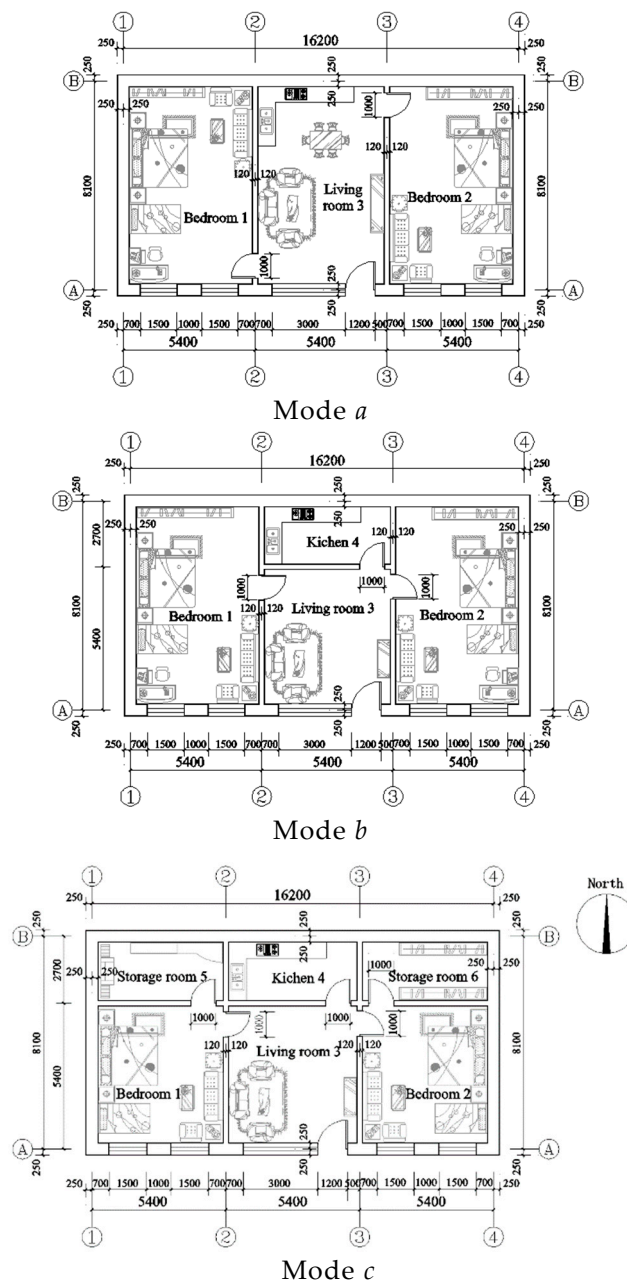


Figure 8. Three indoor space-arrangement modes.

3.2. Mathematical Analysis Model

3.2.1. Heat Balance on the Outer Surface of the Building Envelope

The external surface of the building envelope directly exchanges heat with the outdoor air and is indirectly affected by solar radiation, including direct solar radiation, sky-scattered radiation, the ground reflected radiation, atmospheric long-wave radiation, and ground long-wave radiation. When these factors simultaneously affect the outer surface of the building envelope, the thermal equilibrium equation [34] is:

$$q_S + q_R + q_B + q_g = q_0 + q_{ra} + q_{ca} \tag{1}$$

in which, the q_S , q_R , q_g , q_0 , and q_{ca} are calculated as follows:

$$q_S = \alpha_{D\theta} I_{D\theta} + \alpha_{d\theta} I_{d\theta} \tag{2}$$

$$q_R = \alpha_{d\theta} I_{R\theta} = \alpha_{d\theta} \rho_g I_{SH} (1 - \cos^2 \frac{\theta}{2}) \tag{3}$$

$$q_g = C_b \varepsilon_g \left(\frac{T_g}{100}\right)^4 \varphi_g \tag{4}$$

$$q_{ca} = \alpha_{ca} (t_0 - t_a) \tag{5}$$

$$q_0 = K(t_0 - t_i) \tag{6}$$

Formula (6) is the heat transfer equation of the wall and the direction of heat flow is considered in one-dimensional perpendicular to the wall.

3.2.2. Heat Balance on the Inner Surface of the Building Envelope

The inner surface of the building envelope is subjected to conduction heat, direct radiant heat, and radiant heat between surfaces, and convective transfer heat with indoor air. These heat transfers can be incorporated into a heat balance equation. The general formula is stated as following:

“Conduction heat” + “convective heat of indoor air” + “mutual radiant heat between surfaces” + “direct radiant heat” = 0.

At the moment n , for the unit area on i -th surface, the heat balance equation is:

$$q_i(n) + \alpha_i^0 [t_r(n) - t_i(n)] + \sum_{k=1}^{N_i} C_b \varepsilon_{ik} \varphi_{ik} \left[\left(\frac{T_k(n)}{100}\right)^4 - \left(\frac{T_i(n)}{100}\right)^4 \right] + q_i^r(n) = 0 \tag{7}$$

3.2.3. Thermal Balance of Transparent Building Envelope

The exterior window and door of the building studied in this paper only are equipped with a double glaze. There exist four glazed surfaces in the outer window and door and consequent four heat balance equations. The heat balance equations on the inner surface of the glass are based on the following assumptions: (1) The heat capacity of the glass is ignored since the glass of the window is very thin; (2) the heat flow direction is perpendicular to the glass surface and one-dimensional; (3) the glass surface is opaque for long-wave radiation; (4) the inner and outer surfaces of the glass are isothermal; (5) the heat of short-wave radiation absorbed by the glass is distributed to the inner and outer surfaces in the same proportions. The heat balance equations of four surfaces are as follows:

$$E_0 \varepsilon_1 - \varepsilon_1 \sigma \theta_1^4 + k_1(\theta_2 - \theta_1) + \alpha_0(t_0 - \theta_1) + S_1 = 0 \tag{8}$$

$$k_1(\theta_1 - \theta_2) + h(\theta_3 - \theta_2) + \sigma \frac{\varepsilon_2 \varepsilon_3}{1 - (1 - \varepsilon_2)(1 - \varepsilon_3)} (\theta_3^4 - \theta_2^4) + S_2 = 0 \tag{9}$$

$$h(\theta_3 - \theta_2) + k_2(\theta_4 - \theta_3) + \sigma \frac{\varepsilon_2 \varepsilon_3}{1 - (1 - \varepsilon_2)(1 - \varepsilon_3)} (\theta_2^4 - \theta_3^4) + S_3 = 0 \tag{10}$$

$$E_i \varepsilon_4 - \varepsilon_4 \sigma \theta_4^4 + k_2(\theta_3 - \theta_4) + \alpha_i(t_i - \theta_4) + S_4 = 0 \tag{11}$$

3.2.4. Thermal Balance in Indoor Air

The heat loss disparity in every room results in the difference of indoor air temperatures between rooms in natural operating conditions because the rooms in multi-space solar buildings are arranged at diverse locations. The temperature difference between adjacent rooms forces heat transfer through the wall dividing adjoining spaces. In unit time, the rise of indoor air temperature in a room is related

to radiation heat exchange, convection heat transfer, heat conduction, cold air infiltration, and other factors. An indoor air thermal equilibrium equation is expressed as following:

$$\sum_{k=1}^{N_i} F_k \alpha_k^c [t_k(n) - t_r(n)] + [q_1^c(n) - q_2^c(n)] + L_a(n)(c\rho)_a [t_a(n) - t_r(n)] / 3.6 - HE_s(n) = V(c\rho)_r \frac{t_r(n) - t_r(n-1)}{3.6 \times \Delta\tau} \quad (12)$$

The above formulas cover the heat balance equation of opaque building envelope inner and outer surfaces, transparent building envelope, and indoor air. These equations together constitute the mathematical model of multi-space passive solar buildings. Temperature indicators in every room will be obtained by solving these equations.

4. Influence of Space-Arrangement and Exterior Wall Thermal Resistance on Indoor Air Temperature

It can be seen from the previous analysis that, in the design of passive solar buildings, the main rooms such as the bedroom and the living room are usually arranged in the south orientation, and the auxiliary rooms in the north orientation. The indoor space layout combined with the directional characteristics of solar radiation is conducive to improving the thermal environment of the main room. However, it is worth noting that in multi-space passive solar buildings, there is heat transfer between indoor and outdoor, and between adjacent rooms. Therefore, the indoor air temperature of the multi-space solar buildings is affected by space-arrangement and thermal resistance of exterior walls.

In order to study the coupling influence of the space-arrangement mode and the thermal resistance of envelope on the indoor air temperature, an available computation program needs to be selected and used to implement numerical simulations. Design Builder is the first comprehensive interface simulation software developed for EnergyPlus. Owing to these powerful features, it was chosen as the software for this study. The weather data for the Lassa area was downloaded from the official website of the U.S. Department of Energy [35].

According to the parameters of space-arrangement modes in Figure 8 and Table 2, the building numerical models (Figure 9) for the three space-arrangement modes were established by the software of Design Builder and the indoor air temperature change in each room was analyzed. In addition, since the indoor air temperature is the most important parameter affecting the indoor thermal environment, in order to simplify the analysis and evaluation, the indoor air temperature is adopted as the indoor thermal environment evaluation parameter.

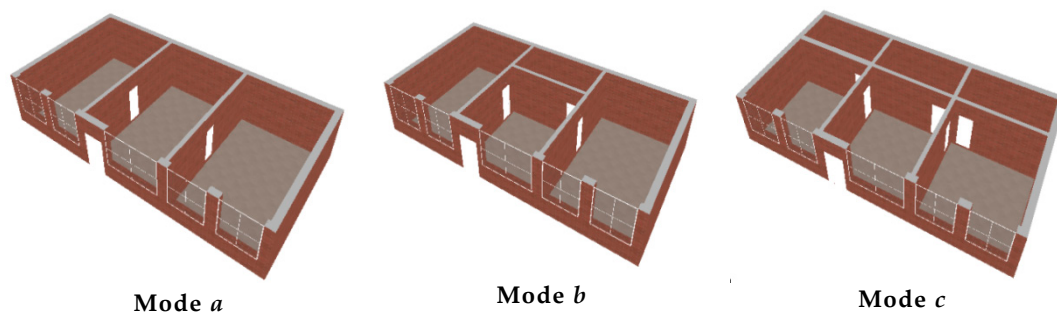


Figure 9. Building numerical models.

The thermal parameters and envelope configuration parameters of the building numerical models are determined based on previous literatures [36,37] and the typical local passive solar building features. The windows are a plastic single-frame and double glazed with the thermal resistance of $0.4 \text{ m}^2 \cdot \text{K}/\text{W}$. The area ratio of the south-facing window to wall is set to 0.5. The thermal resistance of the floor is assigned to $3.3 \text{ m}^2 \cdot \text{K}/\text{W}$. The component and thermal parameters of the building envelope are listed in Table 3.

Table 3. Component and thermal parameters of the building envelope.

Envelope	Material	Thickness (mm)	Thermal Conductivity (Wm ⁻¹ .K ⁻¹)	Density/(kg m ⁻³)	Thermal Resistance (m ² .K.W ⁻¹)
The exterior wall	Cement mortar	20	0.93	1800	0.53
	Dinas brick	370	1.10	1900	
	Cement mortar	20	0.93	1800	
The partition	Cement mortar	20	0.93	1800	0.48
	Dinas brick	240	1.10	1900	
	Cement mortar	20	0.93	1800	
The roof	Cement mortar protective layer	30	0.93	1800	1.43
	Extruded polystyrene plate insulating layer	30	0.03	30	
	Waterproofing layer (two modified asphalts)	6	0.17	600	
	Cement mortar leveling layer	20	0.93	1050	
	Cement expanded perlite slope making layer	30	0.26	800	
	Reinforced concrete slab	100	1.74	2500	
	Cement mortar plastering	20	0.93	1050	

Note: The thermal resistance of the inner surface of the exterior wall is set to 0.11 m².K.W⁻¹, and that of the outer surface is 0.04 m².K.W⁻¹ [17].

In the numerical simulation analysis, the non-stationary calculation was performed, and the calculation period was determined to three months (1 December to 1 March of the following year). The influence of space-arrangement and wall thermal resistance on the indoor air thermal environment was investigated by analyzing the change of the average indoor air temperature values over the coldest month (January). In this study, the purpose of determining the three-month period of the numerical calculation is to eliminate the influence of the initial conditions in the non-stationary calculation process on the results.

4.1. Influence of the Space-Arrangement Mode on the Indoor Temperature

Space-arrangement modes affect the thermal process of passive solar buildings, and consequently affect the indoor air temperature. According to the parameters in Table 3, the Design Builder software was used to analyze the indoor air temperature in the coldest month (January) of the main room in a multi-space passive solar building. In three space-arrangement modes, the thermal resistances of exterior walls in different orientations were all set to 0.53 m².K/W, and the average calculated indoor air temperature values of the main rooms in January are illustrated in Figure 10.

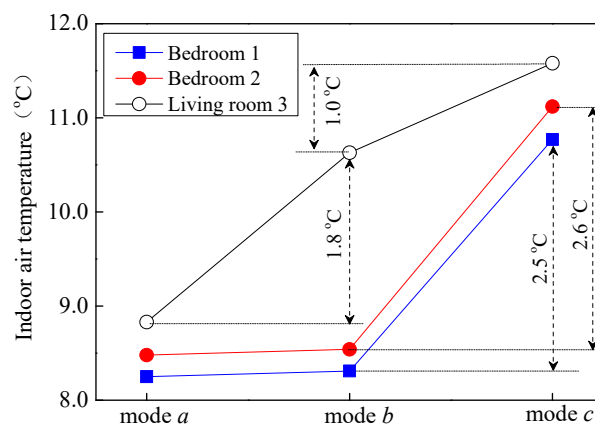


Figure 10. Indoor air temperature of the main rooms in three space-arrangement modes.

Figure 10 indicates that the indoor air temperature of the bedroom and living room in mode c is the highest, followed by that of mode b, while that of mode a is the lowest. Apparently, the indoor

space-arrangement modes have a significant impact on the thermal environment under the same thermal parameters of the building envelope. Compared to 8.8 °C of the indoor air temperature of the living room in the mode *a*, that of living room in the model *b* is 10.6 °C, increased by 20.5%, and the indoor air temperature growth rate of the living room is higher than that of the bedroom. When the space-arrangement mode is changed from mode *b* to mode *c*, the increase rate of the air temperature of the bedroom is higher than that in the living room. The air temperature rise from 8.3 °C to 10.8 °C in bedroom 1, and from 8.5 °C to 11.1 °C in bedroom 2, and from 10.6 °C to 11.6 °C in the living room. It is worth noting that the indoor air temperature of bedroom 1, bedroom 2, and living room has increased by 30.1%, 30.6%, and 9.4%, respectively.

Comparing three space-arrangement modes and corresponding indoor air temperatures of the main rooms, it can be found that the north-facing auxiliary rooms in the model *c* not only enrich the function of the building interior space, but also act as a “temperature buffer” which is beneficial to improve the temperature of the main rooms.

4.2. Influence of Exterior Wall Thermal Resistance on Indoor Air Temperature

Due to the temperature difference between adjacent rooms in a multi-space passive solar building, there is not only heat transfer between indoor and outdoor, but also heat transfer between adjacent rooms. Therefore, the change of the thermal resistance of the exterior wall in different orientations has different effects on the indoor air temperature of each room. It is investigated that, in the space-arrangement mode *c*, the indoor air temperatures of the main rooms varied with the increasing thermal resistance of the exterior walls, and the result is shown in Figure 11.

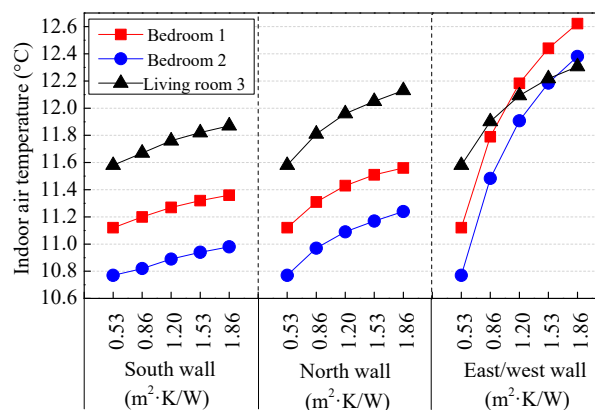


Figure 11. Indoor air temperatures of the main rooms change with the thermal resistance of the exterior walls in mode *c*.

It can be seen from Figure 11 that increasing the same amount of the thermal resistance of different exterior walls has different effects on the indoor air temperature of the main room. The indoor air temperatures of the mode *c* were analyzed under the condition of thermal resistance change of different exterior walls. It is deduced that the indoor air temperature of the mode *c* varies with the thermal resistances of diverse orientation walls. Figure 12 shows the increment of indoor air temperatures of all rooms caused by increasing thermal resistance of exterior walls in different directions.

From Figure 12, it can be seen that the effect of the wall thermal resistance on the indoor air temperature is different even if the thermal resistance of walls in different orientations is equally increased. Through the comparative analysis of Figure 12a–c, it can be found that increasing the thermal resistance of east/west walls can significantly increase the indoor air temperature of the main rooms (living room and bedrooms). However, increasing the thermal resistance of the north wall can increase the indoor air temperature of the auxiliary room more obviously.

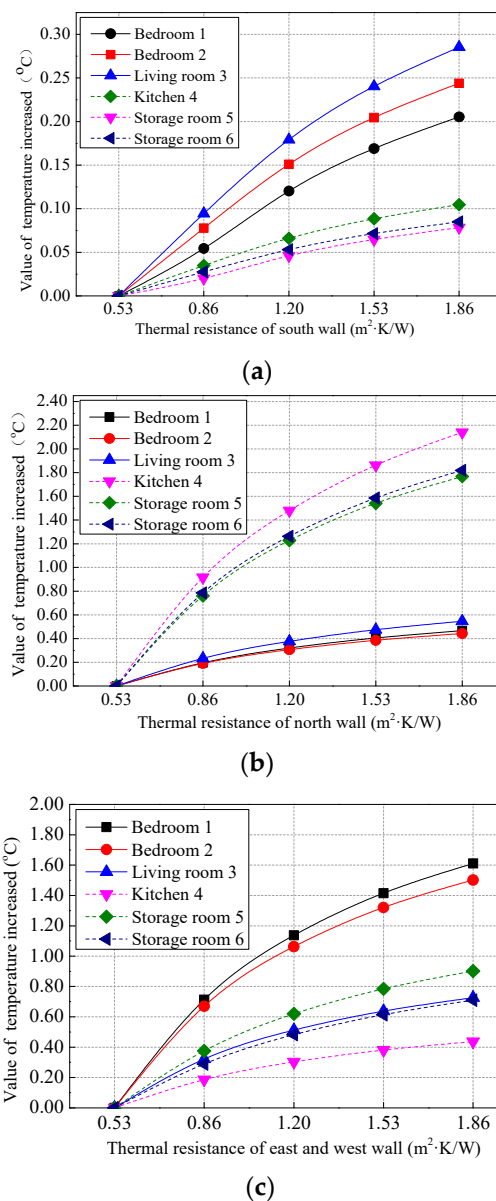


Figure 12. Indoor air temperature increases with the increase of exterior walls thermal resistance. (a) South wall; (b) north wall; (c) east/west wall.

Figure 12a presents that as the thermal resistance of the south wall increases, the indoor air temperature in each room rises slightly, and the temperature rise in the main room is slightly higher than that in the auxiliary room. When the thermal resistance of the south wall increases from $0.53 \text{ m}^2\cdot\text{K/W}$ to $1.86 \text{ m}^2\cdot\text{K/W}$, the indoor air temperature of the living room and bedroom (the average value of indoor air temperature in bedroom 1 and bedroom 2) increases by $0.29 \text{ }^\circ\text{C}$ and $0.22 \text{ }^\circ\text{C}$, and the temperature increment of auxiliary rooms is less than $0.11 \text{ }^\circ\text{C}$. However, under the condition of the same increment of the north wall thermal resistance, the air temperature of the auxiliary rooms increases significantly, while the indoor air temperature of the living room and bedroom only slightly increase by $0.55 \text{ }^\circ\text{C}$ and $0.46 \text{ }^\circ\text{C}$, respectively (Figure 12b). Figure 12c indicates that the same increment of the east/west wall thermal resistance has a greater impact on the indoor air temperature of the main rooms (bedrooms and living room) than those of the south and north walls. When the thermal resistance of the east/west walls is increased from $0.53 \text{ m}^2\cdot\text{K/W}$ to $1.86 \text{ m}^2\cdot\text{K/W}$, the indoor air temperature of the living room and the bedroom increases by $0.73 \text{ }^\circ\text{C}$ and $1.56 \text{ }^\circ\text{C}$, respectively. Comparing with the temperature rise in the living room and bedroom caused by the thermal resistance increasing of the south wall and north

wall, that of the living room caused by the thermal resistance increasing of the east/west wall increases by 151.7% and 32.7%, and that of the bedroom increases by 609.1% and 239.1%, respectively.

The above results show that in the natural working state of multi-space passive solar buildings, there is a significant difference between the heat transfer loss and the passive heat collection in each room, due to the directional characteristics of solar radiation and the complicated heat transfer process between adjacent rooms.

4.3. Influence of Wall Thermal Resistance on Indoor Air Temperature Deference between Main and Auxiliary Rooms

During natural operation, the indoor air temperature of the main room in a passive solar building is mainly affected by two aspects: One is the net amount of solar radiant energy collected by the building; the other is the proportion of heat allocated between the main and auxiliary rooms. The previous analysis results show that even if the thermal resistance of different exterior walls changes by the same amount, the temperature difference between the main and auxiliary rooms is different. Therefore, it is necessary to analyze the change trend of the temperature difference between the main and auxiliary rooms under the thermal resistance increment of exterior walls in different orientations.

Figure 13 illustrates the variation of indoor air temperature difference between main and auxiliary rooms with the thermal resistance increasing of the exterior wall in the indoor space-arrangement mode *c*. To simplify the analysis, the indoor air temperature of the main room is defined as the average indoor air temperature of the bedroom 1, bedroom 2, and living room, and the indoor air temperature of the auxiliary room is defined as the average temperature of the storage room 5, storage room 6, and kitchen. Figure 14 presents the indoor air temperature differences between the main and auxiliary rooms when the thermal resistances of the exterior walls in different orientations are increased from $0.53 \text{ m}^2 \cdot \text{K}/\text{W}$ to $1.86 \text{ m}^2 \cdot \text{K}/\text{W}$.

From Figure 13 it can be found that increasing thermal resistance of the north wall decreases the temperature differences between the main and auxiliary rooms. When the thermal resistance of the north wall is increased from $0.53 \text{ m}^2 \cdot \text{K}/\text{W}$ to $1.86 \text{ m}^2 \cdot \text{K}/\text{W}$, the indoor air temperature differences between the main and auxiliary rooms decline from $6.3 \text{ }^\circ\text{C}$ to $4.9 \text{ }^\circ\text{C}$, and decreases by 22.2%. Due to the temperature increasing of the auxiliary room, the temperature difference between the main and auxiliary rooms decreases with the thermal resistance increasing of the north wall. Compared with the air temperature rise caused by increasing thermal resistance of the south wall and the east/west wall from $0.53 \text{ m}^2 \cdot \text{K}/\text{W}$ to $1.86 \text{ m}^2 \cdot \text{K}/\text{W}$, the thermal resistance increasing of the north wall can increase the indoor air temperature of the auxiliary room by 36.7% and 21.8%. Meanwhile, the temperature values in Figure 14 indicate that the proportion of thermal energy distributed in the main room can be improved by increasing the thermal resistance of the south exterior wall, but the overall indoor thermal environment of the building does not improve significantly. It can be deduced that as the heat transfer loss of the building through the east/west wall decreases with the increase of thermal resistance, the indoor air temperature of the main room increases significantly, while the temperature of the auxiliary room increases slightly. It can be seen from Figure 14 that when the east/west wall adopts the maximum thermal resistance of $1.86 \text{ m}^2 \cdot \text{K}/\text{W}$, the indoor air temperature of the main room is $12.4 \text{ }^\circ\text{C}$, which is 8.8% and 6.9% higher than that of the same thermal resistance of the south wall and the north wall. The above result is attributed to the increase of the east/west wall thermal resistance increasing the net heat gain of the main room, thereby increasing the indoor air temperature of the main room.

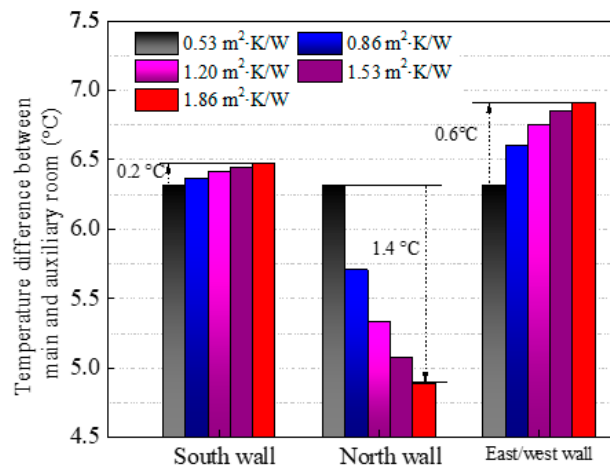


Figure 13. Temperature differences between main and auxiliary rooms caused by increasing the thermal resistance of exterior walls.

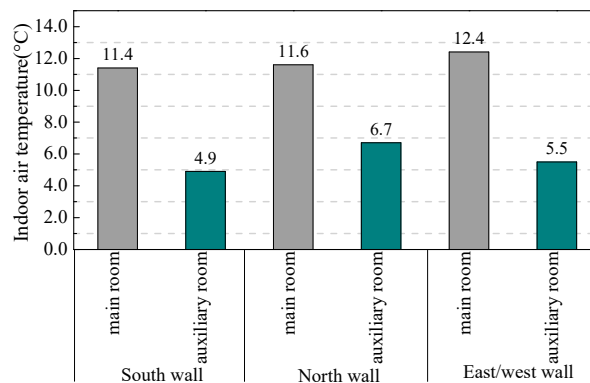


Figure 14. Indoor air temperatures of the main and auxiliary rooms with maximum thermal resistance of exterior walls.

5. Conclusions

- (1) The indoor space-arrangement of passive solar buildings has a significant impact on the air temperature. Through the comparison of indoor air temperature in three modes, it is found that the space-arrangement of “north-south separation” (mode c) not only enriches the building space, but also enables the auxiliary room on the north side to function as a “temperature buffer”, resulting in a higher temperature in the main room. The rationality of the evolution of the indoor space-arrangements of local passive solar buildings has been confirmed by investigation and analysis.
- (2) For the space-arrangement of the “north-south separation” (mode c), increasing the thermal resistance of east/west walls has a significant effect on the indoor air temperature of the main room. Compared with the temperature rise in the living room and bedroom induced by increasing thermal resistance of the south walls and north walls, that of the living room induced by increasing thermal resistance of the east/west walls increases by 151.7% and 32.7%, and that of the bedroom increases by 609.1% and 239.1%, respectively.
- (3) The existence of indoor air temperature difference between the main and auxiliary rooms in the multi-space passive solar building indicates that the optimal distribution of indoor thermal energy in different rooms can be realized through the reasonable design of the building space-arrangement and wall thermal resistance. When the indoor space is arranged as the “north-south separation” (mode c), the effect of equally increasing the thermal resistance of different exterior walls on the indoor air temperature difference between the main and auxiliary rooms is different. Among

them, the thermal resistance increase of the east/west wall leads to the indoor air temperature difference increase, while increasing the thermal resistance of the north wall reduces the indoor air temperature difference between the main and auxiliary rooms.

Author Contributions: Preparing the manuscript, X.C and Y.Z; Methodology, X.C, G.S and Y.Z; Investigation, Y.Z and W.W; Simulation, W.W and L.Z.

Funding: This research was funded by the National Natural Science Foundation of China, grant number [51678482], and the APC was funded by [51678482].

Conflicts of Interest: The authors declare no conflict of interest.

Nomenclature

The following abbreviations are used in this manuscript:

C_b	Black-body radiation constant, Equal to $5.67 \text{ (W/m}^2\cdot\text{K}^4)$
$(c\rho)_{ar}, (c\rho)_r$	Unit heat capacity of outdoor and indoor air ($\text{kJ/m}^2\cdot\text{K}$)
E_0, E_i	Long wave radiation intensity of the outer and inner surfaces (W/m^2)
F_k	Inner surface area of building envelope (m^2)
h	Heat transfer coefficient of gas between glass layers ($\text{W/m}^2\cdot\text{K}$)
$HE_s(n)$	Heat removal capacity of air conditioning system at “n” moment (W)
$I_{D\theta}, I_{d\theta}$	Direct radiation and sky-scattered radiation absorbed by envelope (W/m^2). For vertical plane, $\theta = 90^\circ$; For horizontal plane, $\theta = 0^\circ$.
$I_{R\theta}$	Ground reflected radiation intensity accepted by an inclined plane with a horizontal inclination of θ (W/m^2)
I_{SH}	Total solar radiation intensity to be accepted by the ground (W/m^2)
K	Heat transfer coefficient of envelope ($\text{W/m}^2\cdot\text{K}$)
k_1, k_2	Heat transfer coefficient of the outer glass and inner glass of a double-glazed window ($\text{W/m}^2\cdot\text{K}$)
$L_a(n)$	Amount of air permeability at “n” moment (m^3/h)
N_i	Total number of inner surfaces of rooms with different building envelopes
q_s	Solar radiation absorbed by the outer surface of the envelope (W/m^2)
q_R	Ground reflected radiant heat absorbed by outer surface of the building envelope (W/m^2)
q_B	Intensity of long wave radiation absorbed by the outer surface (W/m^2)
q_g	Ground radiation heat absorbed by envelope (W/m^2)
q_0	Heat transfer of the outer surface of the envelope to the inner surface (W/m^2)
q_{ca}	Convective heat transfer of the outer surface of the envelope to the surrounding air (W/m^2)
q_{ra}	Amount of heat radiation from the outer surface of the envelope to the surrounding environment (W/m^2)
$q_i(n)$	The amount of heat transfer obtained by i -th inner surface of the building envelope (W/m^2)
$q_i^\tau(n)$	Solar radiation and internal disturbance radiation heat in the inner surface of the i -th building envelope (W/m^2)
$q_1^c(n)$	Heat from illumination, human body heat and device display heat at the n -th moment (W)
$q_2^c(n)$	Room heat loss caused by evaporation of water at “n” moment (W)
S_1, S_2	Radiant intensity absorbed by the outer surface and inner surface of the outer glass of a double-glazed window (W/m^2)
S_3, S_4	Radiant intensity absorbed by the outer surface and inner surface of the inner glass of a double-glazed window (W/m^2)
T_g	Ground temperature (K)
t_a, t_i, t_0	Temperature of outer surface and inner surface of the envelope, and outdoor air temperature (K)
$t_r(n)$	Indoor air temperature (K)

$t_i(n), t_k(n)$	Inner surface temperature of the i -th and k -th building envelope (K)
$t_k(n), t_r(n)$	Temperature of the inner and outer surfaces of the building envelope at “ n ” moment (K)
V	Volume of the room (m^3)
$\alpha_{D\theta}, \alpha_{d\theta}$	Absorptivity of direct solar radiation and the sky- scattering radiation
α_{ca}	Convective heat transfer coefficient of outer surface of building envelope ($W/m^2 \cdot K$)
α_i	Convection heat transfer coefficient of inner surface ($W/m^2 \cdot K$)
α_k^c	Convective heat coefficient of the k inner surface ($W/m^2 \cdot K$)
α_i^0	Convective heat transfer coefficient of inner surface of the i -th building envelope ($W/m^2 \cdot K$)
θ_1, θ_2	Outer surface and inner surface temperature of the outer glass of a double-glazed window (K)
θ_3, θ_4	Outer surface and inner surface temperature of the inner glass of a double-glazed window (K)
ε_g	Ground emissivity respectively
ε_{ik}	Degree of system blackness between the i -th and k -th building envelope, as the product of the blackness of the i -th and k -th surface
ε_i	Long-wave emissivity of the i -th surface
φ_g	Radiation angle coefficient of envelope outer surface to ground. Value is 0.5
φ_{ik}	Radiation angle coefficient of the i -th inner surface of the building envelope to the k -th inner surface
σ	Stephen Boltzmann constant
ρ_g	Average reflectivity of the ground
$\Delta\tau$	Unit time (1 h)

References

1. Wang, Q.; Qiu, H.-N. Situation and outlook of solar energy utilization in Tibet, China. *Renew. Sustain. Energy Rev.* **2009**, *13*, 2181–2186. [[CrossRef](#)]
2. Ping, X.; Jiang, Z.; Li, C. Social and ecological effects of biomass utilization and the willingness to use clean energy in the eastern Qinghai–Tibet plateau. *Energy Policy* **2012**, *51*, 828–833. [[CrossRef](#)]
3. Wei, X.; Yang, P.; Wang, Y. Use of rural energy resources and eco-environmental degradation in Tibet. *J. Environ. Sci.* **2004**, *16*, 1046–1050.
4. Liu, G.; Lucas, M.; Shen, L. Rural household energy consumption and its impacts on eco-environment in Tibet: Taking Taktse county as an example. *Renew. Sustain. Energy Rev.* **2008**, *12*, 1890–1908. [[CrossRef](#)]
5. Fang, Y.; Wei, Y. Climate change adaptation on the Qinghai–Tibetan Plateau: The importance of solar energy utilization for rural household. *Renew. Sustain. Energy Rev.* **2013**, *18*, 508–518. [[CrossRef](#)]
6. Tsoutsos, T.; Frantzeskaki, N.; Gekas, V. Environmental impacts from the solar energy technologies. *Energy Policy* **2005**, *33*, 289–296. [[CrossRef](#)]
7. Martinopoulos, G. Solar energy in buildings. In *Reference Module in Earth Systems and Environmental Sciences*; Elsevier: Amsterdam, The Netherlands, 2016. [[CrossRef](#)]
8. Vassiliades, C.; Kalogirou, S.; Michael, A.; Savvides, A. A Roadmap for the Integration of Active Solar Systems into Buildings. *Appl. Sci.* **2019**, *9*, 2462. [[CrossRef](#)]
9. Li, H.; Ma, W.; Lian, Y.; Wang, X.; Zhao, L. Global solar radiation estimation with sunshine duration in Tibet, China. *Renew. Energy* **2011**, *36*, 3141–3145. [[CrossRef](#)]
10. Chow, T.T. A review on photovoltaic/thermal hybrid solar technology. *Appl. Energy* **2010**, *87*, 365–379. [[CrossRef](#)]
11. Abbassi, F.; Dimassi, N.; Dehmani, L. Energetic study of a Trombe wall system under different Tunisian building configurations. *Energy Build.* **2014**, *80*, 302–308. [[CrossRef](#)]
12. Saadatian, O.; Sopian, K.; Lim, C.H.; Asim, N.; Sulaiman, M.Y. Trombe walls: A review of opportunities and challenges in research and development. *Renew. Sustain. Energy Rev.* **2012**, *16*, 6340–6351. [[CrossRef](#)]

13. Duquesne, M.; Palomo Del Barrio, E.; Godin, A. Nucleation Triggering of Highly Undercooled Xylitol Using an Air Lift Reactor for Seasonal Thermal Energy Storage. *Appl. Sci.* **2019**, *9*, 267. [[CrossRef](#)]
14. Stevanović, S. Optimization of passive solar design strategies: A review. *Renew. Sustain. Energy Rev.* **2013**, *25*, 177–196. [[CrossRef](#)]
15. Kirankumar, G.; Saboor, S.; Ashok Babu, T.P. Investigation of Different Window and Wall Materials for Solar Passive Building Design. *Procedia Technol.* **2016**, *24*, 523–530. [[CrossRef](#)]
16. Kong, W.; Liu, Z.; Yang, Y.; Zhou, C.; Lei, J. Preparation and characterizations of asphalt/lauric acid blends phase change materials for potential building materials. *Constr. Build. Mater.* **2017**, *152*, 568–575. [[CrossRef](#)]
17. Xu, T.; Chen, Q.; Huang, G.; Zhang, Z.; Gao, X.; Lu, S. Preparation and thermal energy storage properties of d-Mannitol/expanded graphite composite phase change material. *Sol. Energy Mater. Sol. Cells* **2016**, *155*, 141–146. [[CrossRef](#)]
18. Liu, J.; Yang, L.; Liu, Y.; Tian, G. Key technological research and application of low energy consumption building design in Tibet. *Eng. Sci.* **2011**, *13*, 40–46.
19. Lei, W.; Feng, Y.; Cao, Y.; Yu, N. Thermal Performance Optimization of Solar Heating Building Envelope in Tibet of China. *J. Civ. Archit. Environ. Eng.* **2013**, *35*, 86–91.
20. Wang, D.; Liu, Y.; Wang, Y.; Liu, J. Design and performance of demonstration house with active solar heating in the Qinghai–Tibet Plateau region. *J. Build. Phys.* **2015**, *40*, 55–76. [[CrossRef](#)]
21. Wei, L.; Dan, L.; Baiyi, L.; Min, Z. Effect Analysis of a Passive Solar House in Tibet. *Aasri Procedia* **2012**, *3*, 619–623. [[CrossRef](#)]
22. He, Q.; Liu, D.L.; Zhang, Q. Indoor Thermal Environments Investigation in Winter of Rural Houses in Yinchuan. *Appl. Mech. Mater.* **2012**, *209–211*, 289–293. [[CrossRef](#)]
23. Yanfeng, L.; Jiaping, L.; Liu, Y.; Jing, L. Measureing study of passive solar house for traditional dwelling building in Lhasa area. *Acta Energy Sol. Sin.* **2008**, *29*, 391–394.
24. Sun, H.; Leng, M. Analysis on building energy performance of Tibetan traditional dwelling in cold rural area of Gannan. *Energy Build.* **2015**, *96*, 251–260. [[CrossRef](#)]
25. Yang, L.; Yan, H.; Xu, Y.; Lam, J.C. Residential thermal environment in cold climates at high altitudes and building energy use implications. *Energy Build.* **2013**, *62*, 139–145. [[CrossRef](#)]
26. Li, L.P. Research on Indoor Thermal Environment of Tibetan Rammed Dwellings. *Adv. Mater. Res.* **2011**, *243–249*, 1995–1999. [[CrossRef](#)]
27. Ministry of housing and urban-rural development of the People’s Republic of China. *Design Standard for Energy Efficiency of Residential Buildings in Severe Cold and Cold Zones*; China Building Industry Press: Beijing, China, 2010; Volume JGJ 26-2010.
28. Sang, G.; Liu, J. Study of energy efficiency envelope configuration of heating residential buildings in solar radiation zone. *Acta Energy Sol. Sin.* **2011**, *32*, 416–422.
29. Monge-Barrio, A.; Sánchez-Ostiz, A. Energy efficiency and thermal behaviour of attached sunspaces, in the residential architecture in Spain. Summer Conditions. *Energy Build.* **2015**, *108*, 244–256. [[CrossRef](#)]
30. Oliveti, G.; Arcuri, N.; De Simone, M.; Bruno, R. Solar heat gains and operative temperature in attached sunspaces. *Renew. Energy* **2012**, *39*, 241–249. [[CrossRef](#)]
31. Wang, D.; Liu, Y.; Jiang, J.; Liu, J. The Optimized Matching of Passive Solar Energy supply and Classroom Thermal Demand of Rural Primary and Secondary School in Northwest China. *Procedia Eng.* **2015**, *121*, 1089–1095. [[CrossRef](#)]
32. Shao, N.; Zhang, J.; Ma, L. Analysis on indoor thermal environment and optimization on design parameters of rural residence. *J. Build. Eng.* **2017**, *12*, 229–238. [[CrossRef](#)]
33. Quan, H.; Wenchao, W.; Jiaping, L.; Liu, Y. Climatic adaptation analysis of vernacular houses of Lhasa by climate consultant. *Build. Sci.* **2017**, *33*, 94–100.
34. Qisen, Y.; Qingzhu, Z. *Thermal Process of Building*; China Building Industry Press: Beijing, China, 1986.
35. Wang, W.; Yuan, M.; Li, Y.-Z.; Li, C. Numerical investigation on the impact of an on-top sunspace passive heating approach for typical rural buildings in northern China. *Sol. Energy* **2019**, *186*, 300–310. [[CrossRef](#)]

36. Ministry of housing and urban-rural development of the People's Republic of China. *Technical Code for Passive Solar Building*; China Building Industry Press: Beijing, China, 2012; Volume JGJ/T 267.
37. Ministry of housing and urban-rural development of the People's Republic of China. Design standard for energy efficiency of rural residential buildings. In *Building Envelope Insulation*; China Building Industry Press: Beijing, China, 2013; Volume GB/T 50824.



© 2019 by the authors. Licensee MDPI, Basel, Switzerland. This article is an open access article distributed under the terms and conditions of the Creative Commons Attribution (CC BY) license (<http://creativecommons.org/licenses/by/4.0/>).